2024 European Control Conference (ECC)
June 25-28, 2024. Stockholm, Sweden

Model-based control with disturbance compensation for a SCR catalyst

Jens Wurm[1], Johannes Huber[2], Michael Url[2] and Frank Woittennek[1]

Abstract— **Heavy-duty gas engines are used in industrial applications as well as to supplement the supply of green energy to meet peak demand for electricity and heat. Compliance with increasingly stringent emissions regulations necessitates the use of exhaust gas aftertreatment systems. In this context, engines equipped with selective catalytic reduction (SCR) catalysts, where nitrogen oxides are reduced using urea, are of particular interest. The paper proposes a model-based approach for controlling the outlet NO_X concentration in such catalysts. A distributed-parameter model for both the thermal and the kinetic subsystems explicitly accounts for the transport phenomena within the catalyst. Feedforward control and observer-based state feedback are based on a lumped-parameter approximation of the model equations. Both the controller and the observer use a linear quadratic (LQ) approach to compute feedback and output injection gains, respectively. In order to achieve stationary accurate tracking despite model uncertainties, the observer is extended to estimate constant disturbances. Experimental validation on a real engine is performed to compare the proposed model-based controller (MBC) with a standard proportional–integral–derivative (PID) controller.**

I. INTRODUCTION

The increasing use of renewable energy systems currently requires the use of heavy-duty diesel engines, or due to lower raw emissions preferable gas engines, to cover peak loads. Reducing NO_X emissions is one of the main challenges when using such engines. Numerous recent developments have led to significant improvements in this regard [1], [2] and the use of SCR catalysts is among the most appealing approaches. Various control strategies have been proposed for this type of aftertreatment. An overview of these strategies, including a discussion of the respective advantages and limitations, can be found in [3].

The goal of complying with current and future emission limits is one of the main motivations for this work. This requires control concepts that can maintain specified NO_X concentrations at the outlet of the SCR catalyst even in highly dynamic regimes. Though PID controllers are standard in industrial applications as described in [4], there are several contributions concerning the application of model based control strategies [5]–[8], e.g., model predictive control [9]–[11], or sliding mode control [12].

This contrasts with the automotive sector, where the surface coverage is used as the control output, as described among others in [13]. Various control strategies, such as normal and adaptive PID controllers [14], backstepping controllers [5], model-based approaches (physical [15] as well as grey box [16], [17]) have already been tested.

For the case under investigation here, model-based applications have also been investigated [6]–[8], but the authors differ from the approaches presented with the structure they propagate.

Similarly as the above mentioned approaches, the present work proposes a model-based control scheme, called MBC, based on an infinite-dimensional description of the coupled kinetic and thermal behavior. However, in contrast to the former, the thermal model includes an adjusted flow velocity due to the thermal storage capacity of the catalytic cell in connection with its particular geometry. Commonly, the control aim consists in achieving a maximal NO_X reduction while keeping a desired mean NH_3 slip [18]. In contrast, within this work a NO_X concentration at the outlet shall be maintained while maintaining the best possible fill level of the catalyst.

As usual, the urea flow – respectively the NH_3 concentration – at the inlet constitutes the control input. Moreover, NO_X concentration in the engine exhaust is considered as a measured disturbance.

For the presented control concept, the distributed-parameter models are spatially discretized and linearized around quasi-stationary trajectories. The resulting finite-dimensional linear time-variant model is used for the feed-forward as well as state feedback and observer design. Thereby, the observer is extended by a simple disturbance model in order to ensure accurate tracking, at least in the steady state despite model uncertainties and disturbances. This is essential for industrial applications.

The contribution is structured as follows. The thermal and kinetic distributed-parameter models are presented in Section II including the approximation by finite-dimensional models. Based on this lumped description, Section III describes the control approach and discusses the individual components, i.e., the feed-forward law, the state feedback and the state observer with disturbance estimation. Finally, in Section IV the proposed controller is experimentally validated and compared with a standard PID controller.

II. MODELING

The aftertreatment system under consideration uses an SCR catalyst. During operation, a urea solution is injected into the exhaust gas upstream of the SCR. At high exhaust gas temperatures, the urea is decomposed into CO_2 and NH_3, where the latter is stored in the catalyst. In several

[1]Jens Wurm and Frank Woittennek are with Institute of Automation and Control Engineering, Private University For Health Sciences and Health Technology, Eduard Wallnöfer Zentrum 1, Hall in Tirol, Austria {jens.wurm,frank.woittennek}@umit-tirol.at

[2]Michael Url and Johannes Huber are with INNIO Jenbacher GmbH & Co OG, Jenbach, Austria {johannes.huber,michael.url}@innio.com

SCR reactions, the nitrogen oxides are reduced to N_2 by means of the NH_3. Model-based control design requires real-time capable models which capture the essential phenomena while maintaining the required accuracy. Since the kinetic reactions are temperature-dependent, separate models are used for the thermal and the kinetic behavior. Both parts are modeled as a one-dimensional plug flow of an incompressible medium. The thermal model takes into account the honeycomb structure of the catalytic cell to best represent the delay caused by the energy storage capacity of the ceramic. Figure 1 shows the general geometric structure of the catalyst under investigation. All material parameters are assumed to be spatially and temporally constant. Although the NO_X reduction with ammonia is exothermic, the heat released can be neglected as the nitrogen oxides only make up $0{,}01\,\%$ of the exhaust gas volume and therefore the amount of heat is negligible [19].

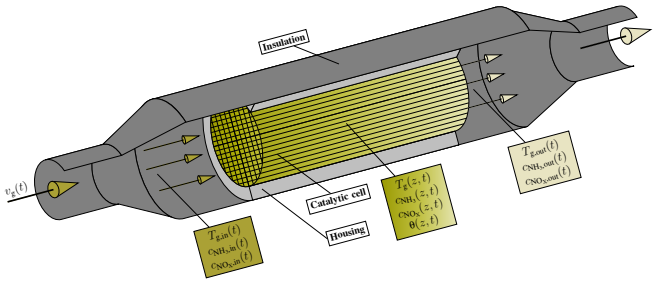

Fig. 1. Schematic of SCR catalyst with in- and output variables as well as considered states.

A. Thermal Model

The ceramic catalyst inside the reactor consists of a number of channels through which the exhaust gas flow is directed, as shown in Figure 2, where the geometric parameters Δx_g, Δy_g of the gas as well as Δx_c, Δy_c of the ceramic layer and the radii for the honeycomb R_g, the separation of housing and isolation R_ws just like the wall closing R_w are explained. This structure must be considered during modeling, as the ceramic absorbs the energy from the exhaust gas flow and thus heats up continuously. As a result, the transport delay of the gas temperature changes massively in relation to the flow velocity. A stainless-steel housing is attached to the outer side, which is surrounded by insulation. Both material layers are not considered individually but are combined to form an overall wall layer. Firstly, the section describes the derivation of the gas temperature model followed by the description of the dynamics of the wall layer. In contrast to existing approaches, such as in [3], the geometric structure and the ceramic material parameters of the catalytic cell are also taken into account, so that the transport velocity and the resulting time delay are appropriately adjusted.

1) Gas-ceramic structure: Based on the honeycomb structure, the different layers are considered separately. The gas temperature $T_{\mathrm{g},i,j}$ of the gas channel i, j can be modeled by the one-dimensional transport equation

$$\begin{aligned} &A_\mathrm{g}\rho_\mathrm{g}c_\mathrm{p,g}\Big(v_\mathrm{g}(t)\partial_z T_{\mathrm{g},i,j}(z,t) + \partial_t T_{\mathrm{g},i,j}(z,t)\Big) \\ &= \alpha_\mathrm{gc}\Delta x_\mathrm{g}\Big(T_{\mathrm{c},i,j+1/2}(z,t) - 2T_{\mathrm{g},i,j}(z,t) + T_{\mathrm{c},i,j-1/2}(z,t)\Big) \\ &+ \alpha_\mathrm{gc}\Delta y_\mathrm{g}\Big(T_{\mathrm{c},i+1/2,j}(z,t) - 2T_{\mathrm{g},i,j}(z,t) + T_{\mathrm{c},i-1/2\,j}(z,t)\Big) \end{aligned} \tag{1}$$

using the model described in [20] with the specific heat capacity $c_\mathrm{p,g}$, the mass density ρ_g of the gas and the cross-section area $A_\mathrm{g} = \Delta x_\mathrm{g}\Delta y_\mathrm{g}$ of a channel as well as the heat transfer coefficient α_gc between the gas and the ceramic. The positive time-varying velocity is denoted by $v_\mathrm{g}(t)$. The boundary condition (BC) is given by the engine outlet temperature witn $T_{\mathrm{g},i,j}(0,t) = T_{\mathrm{g},i,j,\mathrm{in}}(t)$ and the initial condition (IC) follows from $T_{\mathrm{g},i,j}(z,0) = T_{\mathrm{g},i,j,0}(z)$. Neglecting the heat flux in axial direction, the temperature distribution $T_{\mathrm{c},i-1/2,j}$ within the ceramic layer $i-1/2, j$ can be described similarly to the wall model of [20] by the one-dimensional equation

$$\begin{aligned} &A_\mathrm{c}\rho_\mathrm{c}c_\mathrm{p,c}\partial_t T_{\mathrm{c},i-1/2,j}(z,t) \\ &= \Delta y_\mathrm{g}\alpha_\mathrm{gc}\Big(T_{\mathrm{g},i-1,j}(z,t) - 2T_{\mathrm{c},i-1/2,j}(z,t) + T_{\mathrm{g},i,j}(z,t)\Big). \end{aligned} \tag{2}$$

Above, the material parameters of the ceramic are the heat capacity $c_\mathrm{p,c}$, the mass density ρ_c and the cross-section area $A_\mathrm{c} = \Delta x_\mathrm{c}\Delta y_\mathrm{g}$ in x direction resp. $A_\mathrm{c} = \Delta x_\mathrm{g}\Delta y_\mathrm{c}$ in y direction. Adding (1) and (2) reveals the description

$$\begin{aligned} &c_\mathrm{p,gc}\rho_\mathrm{gc}\partial_t\hat{T}_{\mathrm{gc},i,j}(z,t) + \bar{v}_\mathrm{g}(t)\partial_z\hat{T}_{\mathrm{gc},i,j}(z,t) \\ &= \frac{\lambda_\mathrm{gc,x}}{\Delta x_\mathrm{g}^2}\Big(\hat{T}_{\mathrm{gc},i+1,j}(z,t) - 2T_{\mathrm{gc},i,j}(z,t) + \hat{T}_{\mathrm{gc},i-1,j}(z,t)\Big) \\ &+ \frac{\lambda_\mathrm{gc,y}}{\Delta y_\mathrm{g}^2}\Big(\hat{T}_{\mathrm{gc},i,j+1}(z,t) - 2\hat{T}_{\mathrm{gc},i,j}(z,t) + \hat{T}_{\mathrm{gc},i,j-1}(z,t)\Big). \end{aligned}$$

Therein, it has been assumed that

$$\begin{aligned} T_{\mathrm{g},i,j} &= T_{\mathrm{c},i+1/2,j} = T_{\mathrm{c},i,j+1/2} = \hat{T}_{\mathrm{gc},i,j} \\ T_{\mathrm{g},i-1,j} &= T_{\mathrm{c},i-1/2,j} = \hat{T}_{\mathrm{gc},i-1,j} \\ T_{\mathrm{g},i,j-1} &= T_{\mathrm{c},i,j-1/2} = \hat{T}_{\mathrm{gc},i,j-1}, \end{aligned}$$

i.e., the heat exchange between ceramic layer and gas layer is approximated to be immediate, allowing for the introduction of the combined gas-ceramic temperature $\hat{T}_\mathrm{gc}$. Furthermore, the combined material parameter $c_\mathrm{p,gc}\rho_\mathrm{gc} = c_\mathrm{p,g}\rho_\mathrm{g} + 2\epsilon c_\mathrm{p,c}\rho_\mathrm{c}$, the factor $\epsilon = A_\mathrm{c}/A_\mathrm{g}$, the thermal conductivities $\lambda_\mathrm{gc,x} = \alpha_\mathrm{gc}\Delta x_\mathrm{g}$ and $\lambda_\mathrm{gc,y} = \alpha_\mathrm{gc}\Delta y_\mathrm{g}$ as well as the scaled velocity $v_\mathrm{gc} = \bar{v}_\mathrm{g}/c_\mathrm{p,gc}\rho_\mathrm{gc}$ with $\bar{v}_\mathrm{g} = c_\mathrm{p,g}\rho_\mathrm{g}v_\mathrm{g}$ occur. It can be seen that the right-hand side of the latter equation involves difference quotients of second order w.r.t. x and y. Therefore, taking the limits $\Delta x \to 0, \Delta y \to 0$, introducing the continuous coordinates $(x, y) \in S_\mathrm{gc}$, where $S_\mathrm{gc} = \{(x, y)|x^2 + y^2 < R_\mathrm{g}^2\}$ is the overall cross-section of the ceramic structure. yields the three-dimensional description in cartesian coordinates

$$\begin{aligned} &c_\mathrm{p,gc}\rho_\mathrm{gc}\partial_t\hat{T}_\mathrm{gc}(x,y,z,t) + \bar{v}_\mathrm{g}(t)\partial_z\hat{T}_\mathrm{gc}(x,y,z,t) \\ &\qquad = \lambda_\mathrm{gc}\,\triangle\hat{T}_\mathrm{gc}(x,y,z,t), \end{aligned} \tag{3a}$$

with the Laplace operator $\triangle = \partial_x^2 + \partial_y^2$. Due to the assumed structure of the catalytic cell, it is expected that the thermal

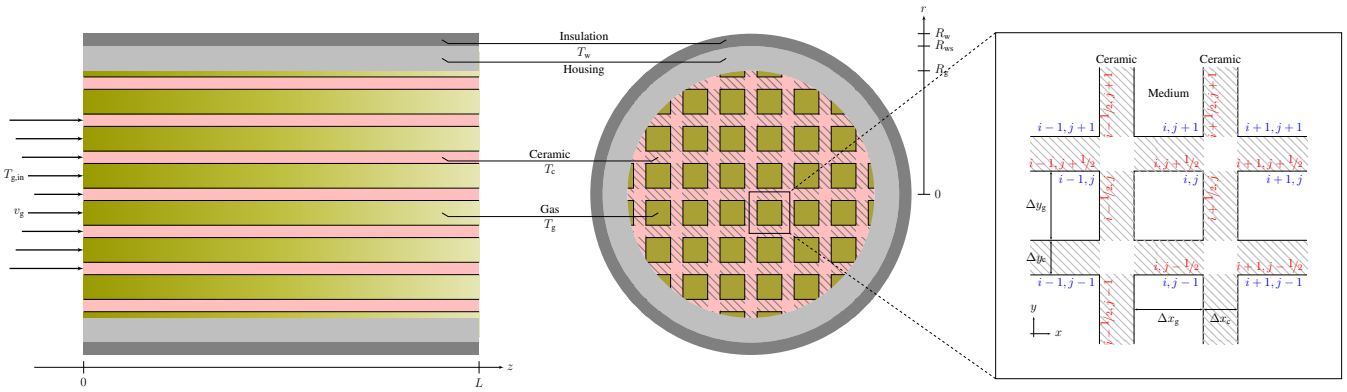

Fig. 2. Front and sectional view with inner honeycomb structure of SCR catalytic cell showing numbered gas and ceramic layers.

conductivity can be summarized as $\lambda_{gc} = \sqrt{\lambda_{gc,x}^2 + \lambda_{gc,y}^2}$. The BC at the inlet follows again from the motor outlet temperature

$$\hat{T}_{gc}(x, y, 0, t) = T_{g,in}(x, y, t), \tag{3b}$$

and the BCs

$$\left\langle \nabla \hat{T}_{gc}(x, y, z, t), \partial \vec{S}_{gc} \right\rangle = \alpha_{gw}\left(T_w(z, t) - \hat{T}_{gc}(x, y, z, t)\right), \tag{3c}$$

for $(x, y) \in \partial S_{gc}$ and the normal unit vector $\partial \vec{S}_{gc}$ at the neighboring housing considering the heat transfer coefficient α_{gw}. The IC is given by $\hat{T}_{gc}(x, y, z, 0) = \hat{T}_{gc,0}(x, y, z)$. Since the three-dimensional model is not manageable in this way, it will be further simplified to a one-dimensional description. For this purpose, the approach used in [20] of averaging the temperature $\hat{T}_{gc}$ over the cross-sectional area S_{gc} with Area $A_{gc} = |S_{gc}| = 2\pi R_g^2$ will be used with

$$T_{gc}(z, t) = \frac{1}{A_{gc}} \int_{S_{gc}} \hat{T}_{gc}(x, y, z, t)\, \mathrm{d}y\, \mathrm{d}x. \tag{4}$$

The authors are aware that a temperature profile is formed over the radius even if the flow is uniformly distributed across the cross-sectional area. However, it is assumed that an averaged gas-ceramic temperature is a close approximation of this and the associated error can be neglected for the application considered.

Integrating (3a) over A_{gc} and substituting (3c), the thermal behaviour can be described by the one-dimensional model

$$A_{gc}\left(\rho_{gc} c_{p,gc} \partial_t + \bar{v}_g(t) \partial_z\right) T_{gc}(z, t) = U_{gw} \breve{\alpha}_{gw}\left(T_w(z, t) - T_{gc}(z, t)\right) \tag{5a}$$

with the BC and the IC

$$T_{gc}(0, t) = T_{g,in}(t), \qquad T_{gc}(z, 0) = T_{gc,0}(z) \tag{5b}$$

including the adapted heat transfer coefficient $\breve{\alpha}_{gw}$, see [20].

The important part of this model adaption comes through scaling of gas velocity v_g with gas and ceramic parameters. The delay time for constant velocities can be calculated by $\tau_g = {}^{L}/_{v_g}$. With the scaled velocity $v_{gc} = {}^{\bar{v}_g}/_{\rho_{gc} c_{p,gc}}$, the delay time $\tau_{gc} = {}^{L}/_{v_{gc}}$ is adapted in a correct way. The validity can be shown by means of measurements as for example in Figure 3. Therein the adapted approach (- - -) and the plug flow model [20] without velocity scaling (-·-·-) are simulated for a measured inlet temperature profile (——) and are compared with a outlet measurement (——) of a catalytic cell[1].

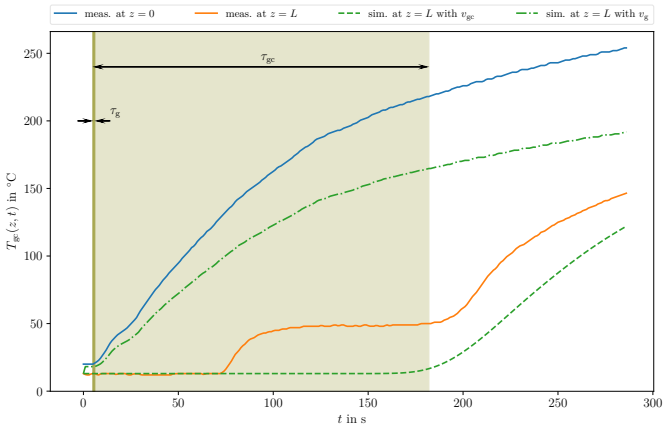

Fig. 3. Comparison of the temperature behavior at the catalyst outlet of the thermal plug flow model -·-·- without velocity scaling from [20] and the velocity adapted model - - -, (5), with a measurement —— at constant speed.

2) Housing: Following the same approach as described for the ceramic layer, the temperature distribution of the housing T_w can be modeled by the one-dimensional equation

$$A_w \rho_w c_{p,w} \partial_t T_w(z, t) = U_{gw} \breve{\alpha}_{gw}\left(T_{gc}(z, t) - T_w(z, t)\right) + U_{g\infty} \alpha_{w\infty}\left(T_\infty(z, t) - T_w(z, t)\right) \tag{5c}$$

using the average wall temperature T_w over the area $A_w = (R_w^2 - R_g^2)\pi$ as well as the average gas-ceramic temperature (4) with the overall heat transfer coefficients $\breve{\alpha}_{gw}$ and $\alpha_{g\infty}$ and the perimeters $U_{gw} = 2\pi R_g$ and $U_{w\infty} = 2\pi R_w$. The heat capacity $c_{p,w}$ and the density ρ_w combine the material values of the insulation and the housing. The IC reads $T_w(z, 0) = T_{w,0}(z)$.

[1]The step in temperature at $t = 80\,\mathrm{s}$ in —— is due to macroscopic effects within the cell and is not modeled. The increase after $t = 180\,\mathrm{s}$ is decisive for the transport phenomenon.

B. Kinetic Model

Approximating the convection through the catalyst by means of a plug flow, the reaction of a species with concentration $c_\bullet$ can be described by means of a one-dimensional convection-reaction

$$\partial_t c_\bullet(z,t) - v_\mathrm{g}(t)\partial_z c_\bullet(z,t) = -\varrho(z,t)$$

including the cumulative reaction rate $(z,t) \mapsto \varrho(z,t)$ of the individual reactions and the flow velocity v_g, which is the same as in (1). Since the system under investigation uses the Eley-Rideal mechanism, all reactions depend on the stored reactant. The temperature dependent storage capacity of the reactant $T_\mathrm{gc} \mapsto \Omega(T_\mathrm{gc})$ is denoted by

$$\Omega\big(T_\mathrm{gc}(z,t)\big) = k_\Omega\, e^{-E_\Omega T_\mathrm{gc}(z,t)}$$

following [21] by using the pre-exponential factor k_Ω and the exponential factor E_Ω. For the description of the actual charge of the catalyst, the surface coverage θ is used, the dynamics of which can be described by the one-dimensional reaction equation

$$\partial_t\theta(z,t) = \frac{1}{\Omega(T_\mathrm{gc})}\left(\varrho_\mathrm{a}(z,t) - \sum_{*}\varrho_*(z,t)\right), \theta(z,t_0) = \theta_0(z)$$

whereby ϱ_a denotes the absorption respectively storage reaction rate. The reaction rate $\varrho = r(b(T_\mathrm{gc}), \Omega(T_\mathrm{gc}), c_\bullet, \theta)$ occurring in the preceding equations is, w.r.t. the exhaust aftertreatment system, a function of the concentrations $c_\bullet$, the coverage θ, the temperature dependent storage capacity Ω and reaction speed $T_\mathrm{gc} \mapsto b(T_\mathrm{gc})$. Unless explicitly stated otherwise, b is given by the Arrhenius equation

$$b\big(T_\mathrm{gc}(z,t)\big) = k\, e^{-\frac{E}{R\,\vartheta_\mathrm{gc}(z,t)}}$$

using the pre-exponential factor k, the activation energy E, the universal gas constant R and the absolute gas-ceramic temperature $\vartheta_\mathrm{gc} = T_\mathrm{gc} + 273{,}15\,^\circ\mathrm{C}$.

For the reduction of exhaust gases four main reactions are considered in the model. Firstly the ammonia (NH_3) absorption $r_\mathrm{a} = \Omega(T_\mathrm{gc})b_\mathrm{a}(T_\mathrm{gc})c_{\mathrm{NH_3}}(1-\theta)$ and desorption reactions $r_\mathrm{d} = -\Omega(T_\mathrm{gc})b_\mathrm{d}(T_\mathrm{gc})\theta$ are the important reactions inside the catalyst and defines the equilibrium of the reaction

$$\mathrm{NH_3 + S} \longleftrightarrow \mathrm{NH_3(S)}.$$

In the process, NH_3 accumulates at the free sites S of the catalyst. The amount of ammonia absorbed is denoted by $NH_3(S)$. To reduce the nitrogen oxides, the *Standard SCR* reaction

$$\mathrm{4\,NH_3(S) + 4\,NO_X + O_2} \longrightarrow \mathrm{4\,N_2 + 6\,H_2O}$$

with the first order reaction rate $r_\mathrm{std} = \Omega(T_\mathrm{gc})b_\mathrm{std}(T_\mathrm{gc})c_{\mathrm{NO_X}}\theta$ ist taken into account. In addition, for high temperatures an oxidation of ammonia to N_2 by

$$\mathrm{4\,NH_3(S) + 3\,O_2} \longrightarrow \mathrm{2\,N_2 + 6\,H_2O}.$$

is also taken under consideration using the first order reaction rate $r_\mathrm{ox} = \Omega(T_\mathrm{gc})b_\mathrm{ox}(T_\mathrm{gc})\theta$. With the presented reactions and the modelling of the individual reaction already introduced at the beginning of the section, the individual transport equations for the species to be investigated can be specified. It reveals the one-dimensional transport system

$$\partial_t c_{\mathrm{NH_3}}(z,t) + v_\mathrm{g}(t)\partial_z c_{\mathrm{NH_3}}(z,t) = \boldsymbol{f}_1(c_{\mathrm{NH_3}}, \theta, T_\mathrm{gc}) \tag{6a}$$
$$\partial_t c_{\mathrm{NO_X}}(z,t) + v_\mathrm{g}(t)\partial_z c_{\mathrm{NO_X}}(z,t) = \boldsymbol{f}_2(c_{\mathrm{NO_X}}, \theta, T_\mathrm{gc}) \tag{6b}$$

with the functions

$$\boldsymbol{f}_1 = -\Omega(T_\mathrm{gc})\Big(b_\mathrm{a}(T_\mathrm{gc})c_{\mathrm{NH_3}}(z,t)\,(1-\theta(z,t)) - b_\mathrm{d}(T_\mathrm{gc})\theta(z,t)\Big)$$
$$\boldsymbol{f}_2 = -\Omega(T_\mathrm{gc})b_\mathrm{std}(T_\mathrm{gc})c_{\mathrm{NO_X}}(z,t)\theta(z,t)$$

for the kinetic behaviour. The change of surface coverage with the previous reactions and the oxidation of ammonia leads to

$$\partial_t\theta(z,t) = g(c_{\mathrm{NH_3}}, c_{\mathrm{NO_X}}, \theta, T_\mathrm{gc}) \tag{6c}$$

with

$$g = b_\mathrm{a}(T_\mathrm{gc})c_{\mathrm{NH_3}}(z,t) - \Big(b_\mathrm{a}(T_\mathrm{gc})c_{\mathrm{NH_3}}(z,t) + b_\mathrm{d}(T_\mathrm{gc}) + b_\mathrm{std}(T_\mathrm{gc})c_{\mathrm{NO_X}}(z,t) + b_\mathrm{ox}(T_\mathrm{gc})\Big)\theta(z,t).$$

The system includes the BCs and ICs

$$c_{\mathrm{NH_3}}(0,t) = c_{\mathrm{NH_3,in}}(t), \quad c_{\mathrm{NO_X}}(0,t) = c_{\mathrm{NO_X,in}}(t) \tag{6d}$$
$$c_{\mathrm{NH_3}}(z,t_0) = c_{\mathrm{NH_3},0}(z), \quad c_{\mathrm{NO_X}}(z,t_0) = c_{\mathrm{NO_X},0}(z), \tag{6e}$$
$$\theta(z,t_0) = \theta_0(z). \tag{6f}$$

As described in [22, Chap. 4.2], it can be assumed that the processes within the gas phase take place much faster than the storage of the thermal energy as well as the accumulation of the ammonia on the catalyst surface. This aspect has already been demonstrated by the derivation of the substitute thermal model (5) in Section II-A. Therefore, the transport processes (6a)-(6b) are considered stationary w.r.t. time. It results the final description

$$v_\mathrm{g}(t)\partial_z c_{\mathrm{NH_3}}(z,t) = \boldsymbol{f}_1(c_{\mathrm{NH_3}}, \theta, T_\mathrm{gc}) \tag{7a}$$
$$v_\mathrm{g}(t)\partial_z c_{\mathrm{NO_X}}(z,t) = \boldsymbol{f}_2(c_{\mathrm{NO_X}}, \theta, T_\mathrm{gc}) \tag{7b}$$

with (6c) and the BCs (6d) as well as the ICs (6f).

C. Discretization

An early lumping approach is used for control design. To this end, approximations of the partial differential equation (PDE) models (5) and (7) are obtained by spatial discretization via the finite difference method (FDM), using backward differences to approximate the derivatives:

$$(\partial_z q)(z_i,t) \approx \tfrac{q_i(t)-q_{i-1}(t)}{\Delta z}, \qquad q_i(t) = q(z_i,t). \tag{8}$$

Above, the $N+1$ sampling points $0 = z_0, \ldots, z_N = L$ are assumed to be equally distributed, i.e., $\Delta z = z_N/N$. This procedure yields a system of ordinary differential equations (ODEs) w.r.t. time for both the thermal and kinetic model. In a second step, the obtained ODE models are discretized w.r.t. time by means of an explicit Euler method.

1) Thermal model: Spatial discretization of the thermal model (5) according to the above described procedure results in a linear time-variant state-space representation

$$\dot{\boldsymbol{x}}_{\mathrm{T}}(t) = \mathbf{A}_{\mathrm{T}}(t)\boldsymbol{x}_{\mathrm{T}}(t) + \mathbf{B}_{\mathrm{T}}(t)\boldsymbol{d}_{\mathrm{T}}(t), \quad \boldsymbol{x}_{\mathrm{T}}(t_0) = \boldsymbol{x}_{\mathrm{T},0}, \tag{9}$$

with the state vector

$$\boldsymbol{x}_{\mathrm{T}} = \big(T_{\mathrm{gc},1}, \ldots, T_{\mathrm{gc,N}}, T_{\mathrm{w},0}, \ldots, T_{\mathrm{w,N}}\big)^{\mathsf{T}} \in \mathbb{R}^{2N-1},$$

and the input $\boldsymbol{d}_{\mathrm{T}} = \big(T_{\mathrm{g,in}}, T_{\infty}\big)^{\mathsf{T}} \in \mathbb{R}^2$ consists of the ambient and the inlet gas temperatures both considered as known disturbances. The time dependence of the system matrices $\mathbf{A}_{\mathrm{T}}(t) \in \mathbb{R}^{(2N-1)\times(2N-1)}$, $\mathbf{B}_{\mathrm{T}}(t) \in \mathbb{R}^{(2N-1)\times 2}$ is solely a consequence of the varying flow velocity. The discrete time approximation of system (9) is given by

$$\boldsymbol{x}_{\mathrm{T},p+1} = \mathbf{A}_{\mathrm{T},p}\boldsymbol{x}_{\mathrm{T},p} + \mathbf{B}_{\mathrm{T},p}\boldsymbol{d}_{\mathrm{T},p}. \tag{10}$$

with $\mathbf{A}_{\mathrm{T},p} = \mathbf{I} + \Delta t\mathbf{A}_{\mathrm{T}}(t_p)$, $\mathbf{B}_{\mathrm{T},p} = \Delta t\mathbf{B}_{\mathrm{T}}(t_p)$, and constant sampling time $\Delta t = t_{p+1} - t_p$.

2) Kinetic model: In contrast to the thermal model, the kinetic part involves the non-linear reaction rates, which, moreover, depend on the temperatures in $\boldsymbol{x}_{\mathrm{T}}$ of the thermal model. A spatial discretization of (7) using backward differences yields the non-linear semi-explicit differential algebraic equation (DAE)

$$0 = \tilde{\boldsymbol{f}}(\boldsymbol{x}_{\mathrm{K}}, \boldsymbol{z}_{\mathrm{K}}, u_{\mathrm{K}}, d_{\mathrm{K}}, \boldsymbol{x}_{\mathrm{T}}, v_{\mathrm{g}}) \tag{11a}$$

$$\dot{\boldsymbol{x}}_{\mathrm{K}}(t) = \tilde{g}(\boldsymbol{x}_{\mathrm{K}}, \boldsymbol{z}_{\mathrm{K}}, \boldsymbol{x}_{\mathrm{T}}), \qquad \boldsymbol{x}_{\mathrm{K}}(t_0) = \boldsymbol{x}_{\mathrm{K},0} \tag{11b}$$

with the state $\boldsymbol{x}_{\mathrm{K}} \in \mathbb{R}^N$ consisting of the spatial discretized surface coverage and the algebraic state $\boldsymbol{z} \in \mathbb{R}^{2N}$ composed of the concentrations of the species NH_3 and NO_X at the discretization points:

$$\boldsymbol{x}_{\mathrm{K}} = \big(\theta_1, \ldots, \theta_{\mathrm{N}}\big)^{\mathsf{T}},$$
$$\boldsymbol{z}_{\mathrm{K}} = \big(c_{\mathrm{NH_3},1}, \ldots, c_{\mathrm{NH_3,N}}, c_{\mathrm{NO_X},1}, \ldots, c_{\mathrm{NO_X,N}}\big)^{\mathsf{T}}.$$

Furthermore, the control input $u_{\mathrm{K}}(t) = c_{\mathrm{NH_3,in}}(t)$ is the NH_3 concentration, while the NO_X concentration at the inlet $d_{\mathrm{K}}(t) = c_{\mathrm{NO_X,in}}(t)$ is considered a disturbance. Again, discretization w.r.t. time is performed by the explicit Euler method, yielding

$$0 = \tilde{\boldsymbol{f}}(\boldsymbol{x}_{\mathrm{K},p}, \boldsymbol{z}_{\mathrm{K},p}, u_{\mathrm{K},p}, d_{\mathrm{K},p}, \boldsymbol{x}_{\mathrm{T},p}, v_{\mathrm{g},p}) \tag{12a}$$

$$\boldsymbol{x}_{\mathrm{K},p+1} = \boldsymbol{x}_{\mathrm{K},p} + \Delta t\, \tilde{g}(\boldsymbol{x}_{\mathrm{K},p}, \boldsymbol{z}_{\mathrm{K},p}, \boldsymbol{x}_{\mathrm{T},p}) \tag{12b}$$

For the determination of the controller and observer gains, the system (12) is approximated by an explicit time-varying linear system. The latter can be obtained by tangent linearization around an arbitrary solution trajectory $p \mapsto (\bar{\boldsymbol{x}}_{\mathrm{K},p}, \bar{\boldsymbol{z}}_{\mathrm{K},p}, \bar{u}_{\mathrm{K},p}, \bar{d}_{\mathrm{K},p})$. Introducing

$$\tilde{\boldsymbol{x}}_{\mathrm{K},p} = \boldsymbol{x}_{\mathrm{K},p} - \bar{\boldsymbol{x}}_{\mathrm{K},p}, \qquad \tilde{\boldsymbol{z}}_{\mathrm{K},p} = \boldsymbol{z}_{\mathrm{K},p} - \bar{\boldsymbol{z}}_{\mathrm{K},p},$$
$$\tilde{u}_{\mathrm{K},p} = u_{\mathrm{K},p} - \bar{u}_{\mathrm{K},p}, \qquad \tilde{d}_{\mathrm{K},p} = d_{\mathrm{K},p} - \bar{d}_{\mathrm{K},p},$$

this yields the linear time-varying algebraic difference equation (ADE)

$$0 = \mathbf{A}_{11,p}\tilde{\boldsymbol{x}}_{\mathrm{K},p} + \mathbf{A}_{12,p}\tilde{\boldsymbol{z}}_{\mathrm{K},p} + \mathbf{B}_{11,p}\tilde{u}_{\mathrm{K},p} + \mathbf{B}_{12,p}\tilde{d}_{\mathrm{K},p} \tag{13a}$$

$$\tilde{\boldsymbol{x}}_{\mathrm{K},p+1} = \mathbf{A}_{21,p}\tilde{\boldsymbol{x}}_{\mathrm{K},p} + \mathbf{A}_{22,p}\tilde{\boldsymbol{z}}_{\mathrm{K},p}, \tag{13b}$$

where the involved matrices correspond to the respective (partial) Jacobians of the right hand side of (12). This linearization procedure requires a solution of the non-linear model equations (12) as prerequisite. However, instead of computing an exact solution of these equations, quasi-stationary trajectories are used as an approximation. For given $\bar{\boldsymbol{x}}_{\mathrm{K},p}$, $v_{\mathrm{g},p}$, $c_{\mathrm{NH_3,in},p}$, $c_{\mathrm{NO_X,in},p}$ these are defined as solutions of the algebraic equations:

$$0 = \tilde{\boldsymbol{f}}(\bar{\boldsymbol{x}}_{\mathrm{K},p}, \bar{\boldsymbol{z}}_{\mathrm{K},p}, u_{\mathrm{K},p}, d_{\mathrm{K},p}, \boldsymbol{x}_{\mathrm{T},p}, v_{\mathrm{g},p})$$
$$0 = \tilde{g}(\bar{\boldsymbol{x}}_{\mathrm{K},p}, \bar{\boldsymbol{z}}_{\mathrm{K},p}, \bar{\boldsymbol{x}}_{\mathrm{T},p}).$$

The system (13) can be simplified to an explicit state-space description if $\det(\mathbf{A}_{12,p}) \neq 0$, $\forall t \geq t_0$. To this end $\tilde{\boldsymbol{z}}_p$ is determined from (13a) yielding

$$\tilde{\boldsymbol{z}}_{\mathrm{K},p} = -\mathbf{A}_{12,p}^{-1}\big(\mathbf{A}_{11,p}\tilde{\boldsymbol{x}}_{\mathrm{K},p} + \mathbf{B}_{11,p}\tilde{u}_{\mathrm{K},p} + \mathbf{B}_{12,p}\tilde{d}_{\mathrm{K},p}\big).$$

Substituting this expression into (13b) leads to the state-space representation

$$\tilde{\boldsymbol{x}}_{\mathrm{K},p+1} = \mathbf{A}_{\mathrm{K},p}\tilde{\boldsymbol{x}}_p + \mathbf{B}_{\mathrm{K},p}\tilde{u}_{\mathrm{K},p} + \mathbf{D}_{\mathrm{K},p}\tilde{d}_{\mathrm{K},p} \tag{14}$$

including the matrices

$$\mathbf{A}_{\mathrm{K},p} = \mathbf{A}_{21,p} - \mathbf{A}_{22,p}\mathbf{A}_{12,p}^{-1}\mathbf{A}_{11,p},$$
$$\mathbf{B}_{\mathrm{K},p} = -\mathbf{A}_{22,p}\mathbf{A}_{12,p}^{-1}\mathbf{B}_{11,p},$$
$$\mathbf{D}_{\mathrm{K},p} = -\mathbf{A}_{22,p}\mathbf{A}_{12,p}^{-1}\mathbf{B}_{12,p}.$$

III. CONTROL DESIGN

In this section the control concept of the MBC is introduced, which shall track a predefined NO_X concentration reference, $t \mapsto y_{\mathrm{r}}(t) = c_{\mathrm{NO_X,out,r}}(t)$, at the catalyst outlet and shall avoid any ammonia slip, which is a standard problem in the control of large gas-fired power plants. To reduce NO_X, urea is injected into the exhaust gas stream of the engine before the catalyst. The amount of urea depends on the NH_3 concentration in the urea-water solution, which is regarded as the control input $t \mapsto u(t) = u_{\mathrm{K}}(t)$. In addition, the catalyst inlet, outlet and the ambient temperature as well as the velocity of the exhaust gas flow are available as measurements. The system is disturbed by the measured NO_X concentration at the engine outlet, which is the inlet, $t \mapsto c_{\mathrm{NO_X,in}}(t)$, to the catalyst system.

The control structure used is shown in Figure 4 and is divided into the three parts: A. a feed-forward law with input u_{FF}, B. a state feedback with input u_{Ctrl} and C. a state observer extended by an input disturbance compensator with input u_{Dist}. Therefore, the control law u is composed by the sum of these three parts. Based on the kinetic model, a feed-forward law is determined at a stationary solution, whose profile serves as the basis for the subordinate state feedback. To obtain the complete state, an observer is required. The state feedback as well as the observer use an LQ approach to determine the corresponding gains.

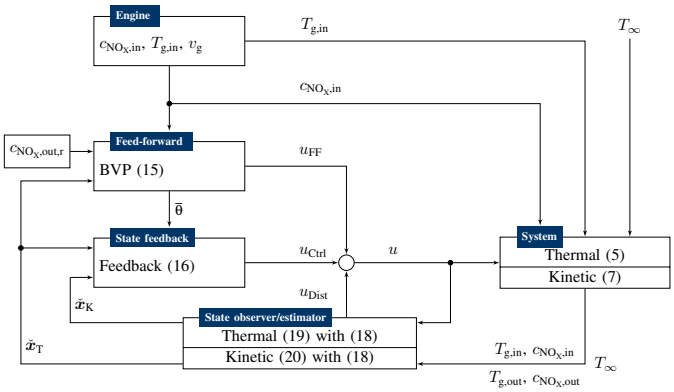

Fig. 4. General control flow overview of MBC.

A. Feed-forward law

To receive a desired $\mathrm{NO_X}$ concentration $t \mapsto y_{\mathrm{r}}(t)$ the input u_{FF} is determined by an inversion-based feed-forward law. Therefore, the non-linear system (7) is considered temporal stationary with the adapted measured BCs

$$c_{\mathrm{NO_X}}(0,t) = c_{\mathrm{NO_X,in}}(t), \quad c_{\mathrm{NO_X,r}}(L,t) = c_{\mathrm{NO_X,out,r}}(t) = y_{\mathrm{r}}(t).$$

To solve this two-point boundary value problem (BVP), the system is discretized w.r.t. space by means of the FDM with the backward difference (8). Thus yields

$$0 = \bar{\boldsymbol{f}}(\bar{\mathbf{c}}_{\mathrm{NH_3}}, \bar{\mathbf{c}}_{\mathrm{NO_X}}, \bar{\theta}, c_{\mathrm{NO_X,in}}, c_{\mathrm{NO_X,out,r}}, \check{\boldsymbol{x}}_{\mathrm{T}}) \tag{15a}$$

$$0 = \bar{g}(\bar{\mathbf{c}}_{\mathrm{NH_3}}, \bar{\mathbf{c}}_{\mathrm{NO_X}}, \bar{\theta}, \check{\boldsymbol{x}}_{\mathrm{T}}), \tag{15b}$$

which is solved for the stationary solutions $\bar{\mathbf{c}}_{\mathrm{NH_3}} = (\bar{c}_{\mathrm{NH_3},0}, \ldots, \bar{c}_{\mathrm{NH_3},N})$ and $\bar{\mathbf{c}}_{\mathrm{NO_X}} = (\bar{c}_{\mathrm{NO_X},1}, \ldots, \bar{c}_{\mathrm{NO_X},N-1})$ as well as $\bar{\theta} = (\bar{\theta}_1, \ldots, \bar{\theta}_N)$ with an iterative method at each time step t. The control input is given by $t \mapsto u_{\mathrm{FF}}(t) = \bar{c}_{\mathrm{NH_3,in}}(t)$. In addition, the medium temperature $\check{\boldsymbol{x}}_{\mathrm{T}}$ is necessary to solve the system, which is provided by an observer, introduced in Section III-C.

B. State feedback design

Since the feed-forward law is based on a temporally stationary design, a controller is necessary to compensate changes of the disturbance and stabilize the system. A state feedback is used for this purpose, as the feed-forward provides the reference profile for the discrete state vector $\bar{\boldsymbol{x}}_{\mathrm{K},p}$ based on the stationary solution of the PDE model. An observer supplies the feedback of the state vector $\boldsymbol{x}_{\mathrm{K},p}$. To specify the controller, the discrete feedback

$$u_{\mathrm{Ctrl},p} = -\boldsymbol{k}_p^{\intercal} \boldsymbol{e}_p, \qquad \boldsymbol{e}_p = \boldsymbol{x}_{\mathrm{K},p} - \bar{\boldsymbol{x}}_{\mathrm{K},p}$$

with the error $\boldsymbol{e} \in \mathbb{R}^N$ and $\bar{\boldsymbol{x}}_{\mathrm{K}} = (\bar{\theta}_1, \ldots, \bar{\theta}_N)^{\intercal} \in \mathbb{R}^N$ is introduced. To determine the gain $\boldsymbol{k}$, a LQ approach is applied by minimizing the cost function

$$J(\boldsymbol{e}, u_{\mathrm{Ctrl}}) = \frac{1}{2} \sum_{i=0}^{O-1} \boldsymbol{e}_i^{\intercal}\, \mathbf{Q}\, \boldsymbol{e}_i + r\, u_{\mathrm{Ctrl},i}^2$$

with the positive definite weighting matrix $0 < \mathbf{Q} \in \mathbb{R}^{N \times N}$ and the positive constant $r \in \mathbb{R}^+$. The solution of the problem can be determined in several ways and is a well-known task, c.f. [23]. The gain $\boldsymbol{k}$ can be determined by means of

$$\boldsymbol{k}_p^{\intercal} = \left(r + \mathbf{B}_{\mathrm{K},p}^{\intercal} \mathbf{S}_{p+1} \mathbf{B}_{\mathrm{K},p}\right)^{-1} \mathbf{B}_{\mathrm{K},p}^{\intercal} \mathbf{S}_{p+1} \mathbf{A}_{\mathrm{K},p} \tag{16a}$$

using the Riccati difference equation (RDE)

$$\mathbf{S}_p = \mathbf{M}_p^{\intercal} \mathbf{S}_{p+1} \mathbf{M}_p + r \boldsymbol{k}_p \boldsymbol{k}_p^{\intercal} + \mathbf{Q} \tag{16b}$$

with $\mathbf{M}_p = \mathbf{A}_{\mathrm{K},p} + \mathbf{B}_{\mathrm{K},p} \boldsymbol{k}_p^{\intercal}$ to determine the stationary solution for $O \to \infty$ at each time step under the condition that the changes of the system matrices can be neglected for future compensation. Thus, for implementation the latter equations are solved iterative at each time step with a fixed iteration count to get the stationary solution.

C. State observer design with disturbance estimation

For feed-forward and state feedback, the current temperature profile of the gas and the current surface coverage are required. Based on a measurement y a generally Luenberger like observer

$$\check{\boldsymbol{x}}_{p+1} = h(\check{\boldsymbol{x}}_p, u_p) + \boldsymbol{l}_p \left(y_p - \mathbf{c}_p^{\intercal} \check{\boldsymbol{x}}_p\right) \tag{17}$$

for any function h is used with the observer state $\check{\boldsymbol{x}}$, the input u and the observer gain $\boldsymbol{l}$. The observer gain is calculated dual to controller design by an LQ approach, which is similar to Kalman filter. Therefore, the discrete system matrix $\mathbf{A}_p$ and the output matrix $\mathbf{c}$ are required from (17). The observer gain $\boldsymbol{l}$ can now be calculated based on

$$\boldsymbol{l}_p = \mathbf{A}_p \mathbf{P}_p \mathbf{c}_p \left(\mathbf{c}_p^{\intercal} \mathbf{P}_p \mathbf{c}_p + r\right)^{-1} \tag{18a}$$

and using the RDE

$$\mathbf{P}_{p+1} = \mathbf{A}_p \mathbf{P}_p \mathbf{A}_p^{\intercal} - \boldsymbol{l}_p \mathbf{c}^{\intercal} \mathbf{P}_p \mathbf{A}_p^{\intercal} + \mathbf{Q} \tag{18b}$$

to get the matrix $\mathbf{P}$.

1) Thermal system: The catalyst outlet gas temperature $y_{\mathrm{T}} = T_{\mathrm{g,out}} = \boldsymbol{x}_{\mathrm{T},N} = \mathbf{c}_{\mathrm{T}}^{\intercal} \boldsymbol{x}_{\mathrm{T}}$, $\mathbf{c}_{\mathrm{T}}^{\intercal} \in \mathbb{R}^{2N-1}$ is available as a measurement. Since (10) is a linear model, the observer follows directly to

$$\check{\boldsymbol{x}}_{\mathrm{T},p} = \mathbf{A}_{\mathrm{T},p} \check{\boldsymbol{x}}_{\mathrm{T},p} + \mathbf{B}_{\mathrm{T},p} \boldsymbol{d}_p + \boldsymbol{l}_{\mathrm{T},p} \left(y_{\mathrm{T},p} - \mathbf{c}_{\mathrm{T}}^{\intercal} \check{\boldsymbol{x}}_{\mathrm{T},p}\right), \tag{19}$$

whereby the observer gain $\boldsymbol{l}_{\mathrm{T}} \in \mathbb{R}^{2N-1}$ is calculated by (18) using $\mathbf{A}_p = \mathbf{A}_{\mathrm{T},p}$ and $\mathbf{c}_p^{\intercal} = \mathbf{c}_{\mathrm{T}}^{\intercal}$.

2) Kinetic system: Similar to the thermal system, the measurement is at the outlet in terms of $\mathrm{NO_X}$ concentration $y_{\mathrm{K}} = c_{\mathrm{NO_X,out}} = \boldsymbol{z}_{\mathrm{K},2N}$. In order to be able to guarantee steady-state accuracy on the real engine, which is not assured by the state feedback used, additionally a disturbance estimation is applied. For this purpose, a constant disturbance ζ_{D} acts on the input u_{K}. This augments the kinetic model (12) to

$$\begin{aligned} 0 &= \tilde{\boldsymbol{f}}(\boldsymbol{x}_{\mathrm{K},p}, \boldsymbol{z}_{\mathrm{K},p}, u_{\mathrm{K},p} + \zeta_{\mathrm{D},p}, d_{\mathrm{K},p}, \boldsymbol{x}_{\mathrm{T},p}, v_{\mathrm{g},p}) \\ \boldsymbol{x}_{\mathrm{K},p+1} &= \boldsymbol{x}_{\mathrm{K},p} + \Delta t\, \tilde{g}(\boldsymbol{x}_{\mathrm{K},p}, \boldsymbol{z}_{\mathrm{K},p}, \boldsymbol{x}_{\mathrm{T},p}) \\ \zeta_{\mathrm{D},p+1} &= \zeta_{\mathrm{D},p} \end{aligned}$$

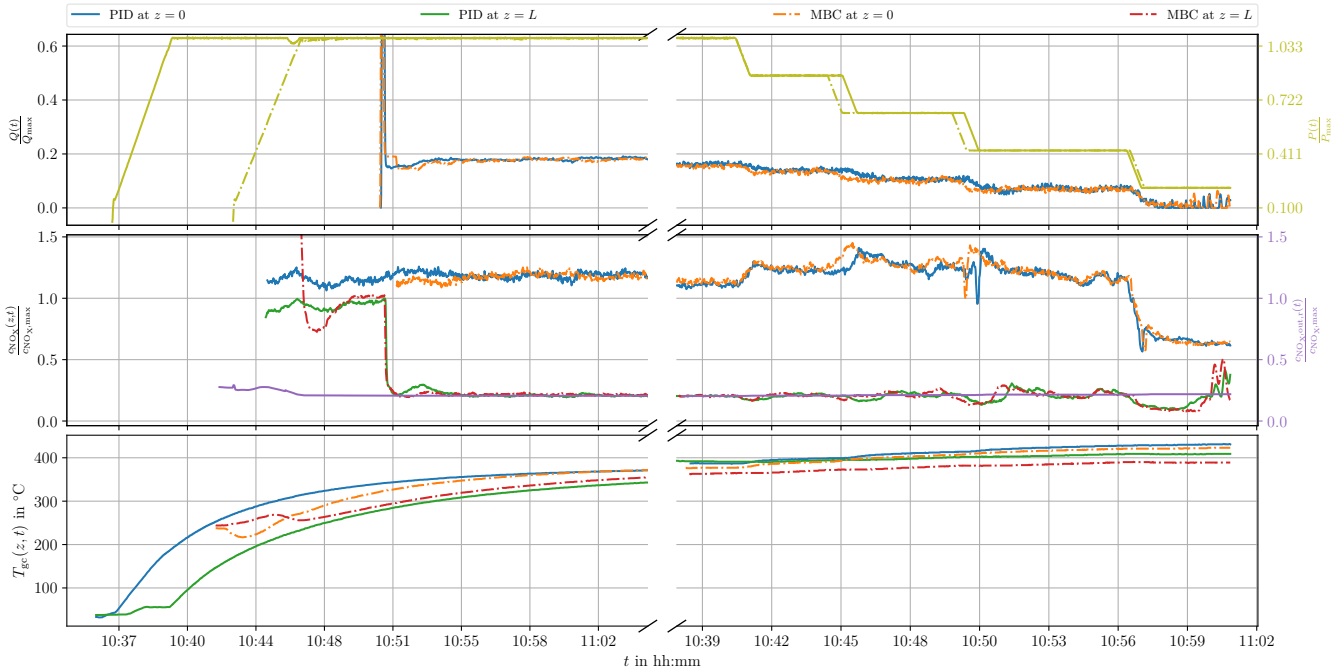

Fig. 5. Comparsion of the outlet NO_X concentration of standard PID controller (——) as well as MBC (-·-·-) to the desired trajectory (——) for similar scenarios.

Based on this description, the observer can now be introduced with

$$0 = \tilde{\boldsymbol{f}}(\check{\boldsymbol{x}}_{\mathrm{K},p}, \check{\boldsymbol{z}}_{\mathrm{K},p}, u_{\mathrm{K},p} + \check{\zeta}_{\mathrm{D},p}, d_{\mathrm{K},p}, \check{\boldsymbol{x}}_{\mathrm{T},p}) \tag{20a}$$

$$\check{\boldsymbol{x}}_{\mathrm{K},p+1} = \check{\boldsymbol{x}}_{\mathrm{K},p} + \Delta t\, \tilde{g}(\check{\boldsymbol{x}}_{\mathrm{K},p}, \check{\boldsymbol{z}}_{\mathrm{K},p}, \check{\boldsymbol{x}}_{\mathrm{T},p}) + \boldsymbol{l}_{\mathrm{K},p}\big(y_p - \check{\boldsymbol{z}}_{\mathrm{K},2N}\big) \tag{20b}$$

$$\check{\zeta}_{\mathrm{D},p+1} = \check{\zeta}_{\mathrm{D},p} + l_{\mathrm{D},p}\big(y_p - \check{\boldsymbol{z}}_{\mathrm{K},2N}\big) \tag{20c}$$

including the observer gain $\tilde{\boldsymbol{l}}_p^{\intercal} = \big(\boldsymbol{l}_{\mathrm{K},p}^{\intercal}, l_{\mathrm{D},p}\big) \in \mathbb{R}^{N+1}$. The gain is calculated according to (18) with

$$\mathbf{A}_p = \begin{pmatrix} \mathbf{A}_{\mathrm{K},p} & \mathbf{B}_{\mathrm{K},p} \\ 0 & 0 \end{pmatrix}, \qquad \mathbf{c}_p^{\intercal} = \begin{pmatrix} \mathbf{c}_{\mathrm{K},p}^{\intercal} & 0 \end{pmatrix},$$

whereby the system matrix $\mathbf{A}_{\mathrm{K},p}$ and input matrix $\mathbf{B}_{\mathrm{K},p}$ are used directly from (14) as well as the output matrix leading to $\mathbf{c}_{\mathrm{K},p}^{\intercal} = \mathbf{c}_{\mathrm{K},\boldsymbol{x},p}^{\intercal} - \mathbf{c}_{\mathrm{K},\boldsymbol{z},p}^{\intercal}\mathbf{A}_{12,p}^{-1}\mathbf{A}_{11,p} \in \mathbb{R}^{N}$ based on relation (13a) and the output relation $y_{\mathrm{K},p} = \begin{pmatrix} 0 & \mathbf{c}_{\mathrm{K},\boldsymbol{z},p}^{\intercal} \end{pmatrix} \begin{pmatrix} \boldsymbol{x}_{\mathrm{K},p} \\ \boldsymbol{z}_{\mathrm{K},p} \end{pmatrix}$.

Finally, the estimated disturbance is lead back to the input by means of

$$u_{\mathrm{Dist},p} = -\check{\zeta}_{\mathrm{D},p} \tag{21}$$

to compensate the disturbances occurring.

IV. Validation

After a successful simulation study, the MBC was applied and used on the exhaust aftertreatment system of an INNIO Jenbacher engine. For the implementation, a spatial grid with $N = 5$ is used for the thermal and kinetic models of the feed-forward, the state feedback as well as the observer. A long-term validation is done. In this context, we will take a closer look at two scenarios, an engine start and a load variation, from this period shown in Figure 5. The MBC is compared against a standard PID controller that uses a simple stoichoiometric feed-forward.

On the left side you can see a standard start-up scenario, where the engine is run to full load. In the upper portion of Figure 5, the load is represented by the normalized power $P(t)/P_{\max}$ shown in ——. Furthermore, the normalized urea flow $Q(t)/Q_{\max}$ is depicted in —— for the PID Regler and in -·-·- for the MBC. First of all, the delay time of the thermal system described in Section II-A is clearly shown in the in- and outlet temperature trends in the lower figure, which result in a temperature difference of up to 70 °C even when the controller is switched on, which means a clear difference in the reaction rates within the catalyst. A delay time of approx. 5 min is clearly visible for both starts. After reaching a limit temperature the controller is enabled and the urea dosing is switched on, which happens at 10:50 for both.

However, it is noticeable that the MBC overshoots significantly less than the PID controller and is already stationary accurate one minute before the PID controller. There is also an overshoot, but it is much smaller compared to the PID controller. The fluctuations of both controllers after transient response are due to the changes of the input NO_X concentration, which shows a comparable process in both cases.

When considering a dynamic load change, which is shown on the right side, both controllers show an almost identical behavior in terms of control quality and dynamics. This shows that the MBC is not subject to any restrictions in relation to the PID controller. In addition, a significantly faster behavior with respect to reaching the steady-state desired value can be seen, especially in the start-up scenario. This contrasts with the adjustability of the weighting factors of the state

feedback and observer, since several measurement and test scenarios have to be carried out for this. It is evident that the MBC has not fully utilized its potential and could be further optimized through additional adjustments.

V. CONCLUSION AND OUTLOOK

Within the paper, a model-based control concept for a SCR catalyst based on distributed-parameter models of the thermal and kinetic subsystem accounting the transport phenomena is presented, which is used to comply with the NO_X emission restrictions. Taking into account the material parameters and the honeycomb geometry, an adapted thermal model was derived which correctly reproduces the delay time. The transport processes of kinetic model can be considered stationary w.r.t. time. Through an implementation on an engine controller, the industrial applicability and a comparable behavior to standard PID controller could be demonstrated. For the next steps, the used stationary feed-forward law should be extended by a dynamic approach as presented by the authors in [24]. This should allow a much better compliance with the desired behavior even in the case of dynamic transitions. Based on this, it makes sense to split the kinetic of the mixed NO_X into NO and NO_2 in order to be able to describe the process more accurately. Currently, the division of the nitrogen oxide concentration does not make sense, as the system is not equipped with the necessary sensors. However, an extension of the algorithms to this end is easily possible. In order to further increase the accuracy of the model, the corresponding peripheral devices in form of urea dosing system and sensor dynamics still has to be taken into account. Finally, engine information is required for dynamic feed-forward, which must be provided by an appropriate engine model. The logical consequence would be to combine the engine controller with exhaust gas aftertreatment in order to take the emissions in consideration during load planning.

REFERENCES

[1] T. Dallmann and L. Jin, "Fuel efficiency and climate impacts of soot-free heavy-duty diesel engines," *International Council on Clean Transportation*, 2020.

[2] T. K. Hansen, "Development of new diesel oxidation and NH3 slip catalysts," Ph.D. dissertation, Technical University of Denmark, 2017.

[3] X. Yuan, H. Liu, and Y. Gao, "Diesel engine SCR control: Current development and future challenges," *Emiss. Control. Sci. Technol.*, 2015.

[4] P. Belli, S. Bittanti, P. Bolzern, M. Campi, A. De Marco, A. Ferretti, S. Malloggi, and W. Prandoni, "A control system for nitrogen oxides pollution abatement by SCR (selective catalytic reduction)," *IFAC Proceedings Volumes*, vol. 29, pp. 6855–6860, 1996.

[5] M.-F. Hsieh, "Control of diesel engine urea selective catalytic reduction systems," Ph.D. dissertation, The Ohio State University, 2010.

[6] J. H. Johnson, G. G. Parker, M. N. Devarakonda, and V. Strots, "Model-based control system design in a urea-SCR aftertreatment system based on NH3 sensor feedback," *Int. J. Automot. Technol.*, 2009.

[7] M. Devarakonda, G. Parker, J. H. Johnson, V. Strots, and S. Santhanam, "Model-based estimation and control system development in a urea-SCR aftertreatment system," *SAE Int. J. Fuels Lubr.*, 2008.

[8] Q. Song and G. Zhu, "Model-based closed-loop control of urea SCR exhaust aftertreatment system for diesel engine," in *SAE Tech. Pap.*, 2002.

[9] S. Stadlbauer, H. Waschl, and L. del Re, "SCR ammonia dosing control by a nonlinear model predictive controller," *IFAC-PapersOnLine*, vol. 47, pp. 3018–3023, 2014.

[10] T. L. McKinley, "Adaptive model predictive control of diesel engine selective catalytic reduction (SCR) systems," Ph.D. dissertation, University of Illinois, 2009.

[11] J. Sowman, D. S. Laila, A. J. Cruden, and P. Fussey, "Nonlinear model predictive control for cold start selective catalytic reduction," *IFAC-PapersOnLine*, vol. 48, pp. 471–476, 2015.

[12] Y. Ma and J. Wang, "Sliding-mode control of automotive selective catalytic reduction systems with state estimation," *Proc. Inst. Mech. Eng. D*, vol. 234, 2019.

[13] F. Willems and R. Cloudt, "Experimental demonstration of a new model-based SCR control strategy for cleaner heavy-duty diesel engines," *IEEE Trans. Control Syst. Technol.*, 2011.

[14] C. E. Romero, "Optimization of SCR control technology for reduced NOx emissions, improved performance and reduced operating expenses," New York State Energy Research and Development Authority, Tech. Rep., 2009.

[15] J. Zhao, Y. Hu, X. Gong, and H. Chen, "Modelling and control of urea-SCR systems through the triple-step non-linear method in consideration of time-varying parameters and reference dynamics," *Trans. Inst. Meas. Control*, 2016.

[16] G. Zanardo, S. Stadlbauer, H. Waschl, and L. del Re, "Grey box control oriented SCR model," in *SAE Tech. Pap.*, 2013.

[17] S. Kannepalli, A. Bürger, S. Tischer, and O. Deutschmann, "Model-based optimization of ammonia dosing in NH3-SCR of NOx for transient driving cycle: Model development and simulation," *Emiss. Control. Sci. Technol.*, 2017.

[18] C. M. Schär, C. H. Onder, and H. P. Geering, "Control of an SCR catalytic converter system for a mobile heavy-duty application," *IEEE Trans. Control Syst. Technol.*, 2006.

[19] J. L. Sorrels, D. D. Randall, K. S. Schaffner, and C. R. Fry, *Selective Catalytic Reduction (SCR) Cost Manual Chapter 7th Edition*, 2016, EPA-HQOAR-2015-0341-0032.

[20] J. Wurm, S. Bachler, and F. Woittennek, "On delay partial differential and delay differential thermal models for variable pipe flow," *Int. J. Heat Mass Transf.*, 2020.

[21] S. Pradhan, "Development of an ammonia reduction after-treatment systems for stoichiometric natural gas engines," Ph.D. dissertation, West Virginia University, 2017.

[22] C. M. Schär, "Control of a selective catalytic reduction process," Ph.D. dissertation, ETH Zürich, 2003.

[23] H. Kwakernaak and R. Sivan, *Linear Optimal Control Systems*. Wiley Interscience, 1972.

[24] J. Wurm and F. Woittennek, "Trajectory planning and control of convection reaction models with storage effects," *IFAC-PapersOnLine*, 2023.